ACS Chemical Neuroscience

Research Article

pubs.acs.org/chemneuro

Differentiating Physicochemical Properties between Addictive and Nonaddictive ADHD Drugs Revealed by Molecular Dynamics Simulation Studies

Panpan Wang,[‡,†] Xiaoyu Zhang,[†] Tingting Fu,[†] Shuang Li,[†] Bo Li,[†] Weiwei Xue,[*,†] Xiaojun Yao,[§] Yuzong Chen,[∥] and Feng Zhu[*,‡,†]

[‡]College of Pharmaceutical Sciences, Zhejiang University, Hangzhou, Zhejiang 310058, China

[†]Innovative Drug Research and Bioinformatics Group, School of Pharmaceutical Sciences and Collaborative Innovation Center for Brain Science, Chongqing University, Chongqing 401331, China

[§]State Key Laboratory of Applied Organic Chemistry and Department of Chemistry, Lanzhou University, Lanzhou 730000, China

[∥]Bioinformatics and Drug Design Group, Department of Pharmacy, National University of Singapore, Singapore 117543, Singapore

Supporting Information

ABSTRACT: Attention-deficit/hyperactivity disorder (ADHD) is the most commonly diagnosed mental disorder of children and adolescents. Although psychostimulants are currently the first-line drugs for ADHD, their highly addictive profile raises great abuse concerns. It is known that psychostimulants' addictiveness is largely attributed to their interaction with dopamine transporter (DAT) and their binding modes in DAT can thus facilitate the understanding of the mechanism underlining drugs' addictiveness. However, no DAT residue able to discriminate ADHD drugs' addictiveness is identified, and the way how different drug structures affect their abuse liability is still elusive. In this study, multiple computational methods were integrated to differentiate binding modes between approved psychostimulants and ADHD drugs of little addictiveness. As a result, variation in energy contribution of 8 residues between addictive and nonaddictive drugs was observed, and a reduction in hydrophobicity of drugs' 2 functional groups was identified as the indicator of drugs' addictiveness. This finding agreed well with the physicochemical properties of 8 officially reported controlled substances. The identified variations in binding mode can shed light on the mechanism underlining drugs' addictiveness, which may thus facilitate the discovery of improved ADHD therapeutics with reduced addictive profile.

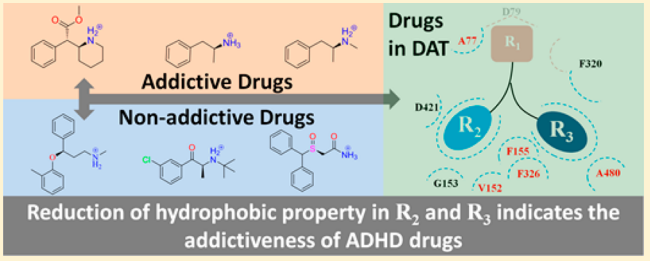

KEYWORDS: *ADHD drug, psychostimulants, addictive profile, abuse potential, molecular dynamics*

INTRODUCTION

As a common neurodevelopmental disease, attention-deficit/hyperactivity disorder (ADHD) seriously affects the daily life of 40 million people,[1] and is estimated to influence 10% of children and 4.5% of adults.[2] Two-thirds of patients diagnosed in childhood show that the disorder persists into adulthood[3] leading to extensive handicap in behavior, emotion, socialization, and career development.[4] As reported, cognitive dysfunctions in ADHD patients are mainly regulated by catecholaminergic signaling in their prefrontal cortex (PFC),[5] and attenuation in PFC's neurotransmission of norepinephrine (NE) and dopamine (DA) has profound effects on ADHD's development.[6−8] Besides of PFC, nucleus accumbens and striatum are also closely associated with ADHD, and elevation of DA in these regions can improve patients' cognitive function.[9]

With the approval of the first selective NE reuptake inhibitor (sNRI) atomoxetine, sNRI was found to be capable of elevating both NE and DA in PFC but with little effect on striatal DA, which made it less effective comparing to another class of ADHD drugs—the psychostimulants.[9−11] Until now, nine ADHD drugs were approved by United States Food and Drug Administration (FDA) and no less than five were in clinical trial (Table 1). Six out of those nine approved drugs were psychostimulants which were prescribed as first-line ADHD medications.[12−14] Psychostimulants elevated catecholamines in regions of not only PFC but also nucleus accumbens and striatum by dual targeting norepinephrine transporter (NET) and dopamine transporter (DAT).[15−17] Both targets were critical,[18,19] which ensured psychostimulants' rapid onset of action and relatively high response rate (~75%) in treating ADHD.[20]

However, one of the major concerns about psychostimulants was their highly addictive profile (with great abuse

Received: May 10, 2017
Accepted: May 30, 2017
Published: May 30, 2017

DOI: 10.1021/acschemneuro.7b00173
ACS Chem. Neurosci. 2017, 8, 1416−1428

Table 1. ADHD Drugs Approved and Tested in Clinical Trial Together with Their Mode of Action, Drug Abuse, and Dependence Information

ADHD drugs approved by FDA						
drug name	trade name	drug mode of action[c]	drug abuse and dependence	company	year	reference[a]
amphetamine	Adderall	NDRI, psychostimulant	schedule II controlled substance	Shire	2001	NDA 021303
atomoxetine	Strattera	sNRI, nonstimulant	not a controlled substance	Lilly	2002	NDA 021411
clonidine	Kapvay	α_2-agonist, nonstimulant	not a controlled substance	Concordia	2009	NDA 022331
dexmethylphenidate	Focalin	NDRI, psychostimulant	schedule II controlled substance	Novartis	2001	NDA 021278
dextroamphetamine	Dexedrine	NDRI, psychostimulant	schedule II controlled substance	Amedra	before 1980	NDA 017078
guanfacine	Intuniv	α_2-agonist, nonstimulant	not a controlled substance	Shire	2009	NDA 022037
lisdexamfetamine	Vyvanse	NDRI, psychostimulant	schedule II controlled substance	Shire	2007	NDA 021977
methamphetamine	Desoxyn	NDRI, psychostimulant	schedule II controlled substance	Recordati	before 1980	NDA 005378
methylphenidate	Ritalin	NDRI, psychostimulant	schedule II controlled substance	Novartis	before 1980	NDA 010187
ADHD drugs in clinical trial development						
Drug name	clinical phase	drug mode of action	drug abuse and dependence	sponsor	study start	reference[b]
bupropion	phase 4	NDRI, nonstimulant	not a controlled substance	CU Denver	2009	NCT00936299
LY2216684	phase 2/3	sNRI, nonstimulant	not a controlled substance	Lilly	2009	NCT00922636
modafinil	phase 2	sDRI, nonstimulant	schedule IV controlled substance	Cephalon	2006	NCT00315276
SPN-812	phase 2	sNRI, nonstimulant	not a controlled substance	Supernus	2016	NCT02633527
SS-reboxetine	phase 2	sNRI, nonstimulant	not a controlled substance	Pfizer	2007	NCT00562055

[a]Information collected from the Drugs@FDA provided by the FDA official Web site. [b]Information collected from the ClinicalTrials.gov provided by the U.S. National Institute of Health. [c]NDRI, norepinephrine−dopamine reuptake inhibitor; sNRI, selective norepinephrine reuptake inhibitor; sDRI, selective dopamine reuptake inhibitor.

potential),[21−24] and this class of drugs was consequently scheduled as controlled substances by the United States Controlled Substances Act.[25] Imaging study demonstrated that attenuation in DA release played key role in people's vulnerability to drug abuse,[26] and the drug−DAT interactions were reported as the major etiology of psychostimulants' addictiveness[27−29] In particular, DAT inhibition controlled dopamine reuptake into presynaptic neuron,[30] and led to the reinforcing effects underling stimulants' addictiveness.[31,32] In contrast, comparing to psychostimulants, various DAT inhibitors treating ADHD (like bupropion and modafinil) showed far milder abuse liability[33,34] indicating that the addictiveness of ADHD drugs could not be simply characterized by the existence of DAT inhibition.[35−37]

DAT inhibitors of different structures were reported to stabilize different DAT conformations, and in turn affected their addictiveness.[38] Particularly, site-directed mutagenesis[39] and cysteine accessibility[38] studies discovered that the DAT conformations stabilized by stimulants and inhibitors with little abuse liability varied.[38] Computational modeling studies, especially molecular dynamics (MD) simulation, had been applied to identify conformation variation induced by ADHD drugs with different degrees of addictiveness[40−42] These computational studies discovered conformation preferentially stabilized by modafinil/bupropion and psychostimulant (methylphenidate),[40,43] which agreed with the findings of experiments[38,39,44] Similarly, the conformation stabilized by another psychostimulant (amphetamine) was simulated and identified as similar to that of psychostimulants.[41] It was known that differences in molecular mode of interaction in DAT between psychostimulants and the drugs of little abuse liability (especially those of clinical importance in Table 1) could help to discover improved and efficacious ADHD drugs.[38,40] However, no study was conducted to identify residues capable of discriminating ADHD drugs' addictiveness, and the way different structures affected the drugs' abuse liability was still elusive. Therefore, it was of great interest to reveal the mechanism underlying the addictiveness of those clinically important (approved or in clinical trial) ADHD drugs.

In this study, a comparative analysis on the modes of interaction between addictive and nonaddictive ADHD drugs was carried out. First, six clinically important drugs were docked into the modeled DAT for MD simulation, and three lines of evidence were provided to verify the simulation results. Second, different modes of interaction between three psychostimulants and three drugs of little addictiveness were identified by variations in per-residue binding energies. Finally, the drugs' key functional groups discriminating their addictiveness were discovered. The identified variations in molecular mode of interaction shed light on mechanism underlining psychostimulants' addictiveness, which may therefore facilitate the discovery of improved therapeutics for ADHD.

RESULTS AND DISCUSSION

Validation of Homology Models and Construction of Drug−Protein Complexes. As shown in Figure S1, >99.6% residues for all constructed models were identified as located in the allowed zone, which indicated the reasonable homology models constructed in this study.[45] Recently, the X-ray structure of human serotonin transporter (hSERT) was solved.[46] On one hand, sequence identity between hSERT and DAT was 52%, which was slightly lower than that (55%) between dDAT[47,48] and DAT. On the other hand, 57% residues of hSERT's S1 binding site (TM1, 3, 6, 8, and 10 regions) were conserved comparing to DAT,[49] which was still lower than that of dDAT (78%). Therefore, the crystal structures of dDAT complexed with various ligands were used to construct homology models of DAT in this study. Here, DAT homology model using hSERT (PDB code 5I6Z)[46] as template was compared with that using dDAT (Figure S2). As illustrated, the structural superimposition between the homology models based on dDAT and hSERT revealed that the binding sites of these 2 models were substantially similar to each other (the majority of RMSD < 1). Although a relatively large RMSD

DOI: 10.1021/acschemneuro.7b00173
ACS Chem. Neurosci. 2017, 8, 1416−1428

Table 2. Calculated and Experimental Binding Energies of six Studied ADHD Drug Binding to Wild Type DAT (ΔG is in kcal/mol and K_i Value is in nM)

ADHD drug	K_i[a]	ΔG_{calc}[b]	$\Delta\Delta G_{exp}$[c]	ΔG_{calc}[d]	$\Delta\Delta G_{calc}$[c]
atomoxetine	1451	−8.275	1.353	−41.31	3.45
dexmethylphenidate	161	−9.628	0	−44.76	0
dextroamphetamine	5680	−7.435	2.193	−34.2	10.56
dextromethamphetamine	1850	−8.126	1.502	−38.12	6.64
R-bupropion	871	−8.589	1.039	−40.78	3.98
R-modafinil	780	−8.657	0.971	−40.7	4.06

[a]Experimental K_i values reported in previous publications.[33,52−55] [b]Estimated binding energy based on K_i values using $\Delta G_{exp} = RT\ln(K_i)$, where R = 8.314J/(mol·K) and T = 310 K. [c]Binding energy difference was computed using $\Delta\Delta G = \Delta G - \Delta G_{dexmethylphenidate}$. [d]Calculated binding energy in this work.

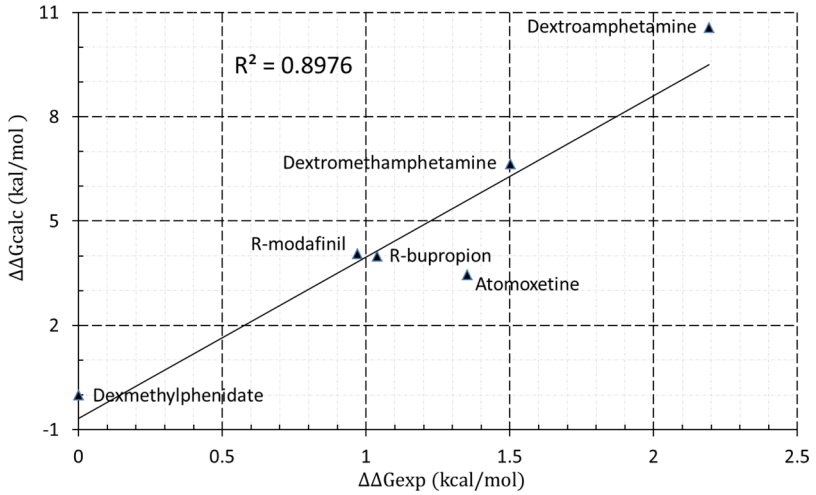

Figure 1. Graphical representation of correlation between the binding energy differences of simulation ($\Delta\Delta G_{calc}$) and that of experiment ($\Delta\Delta G_{exp}$) for six studied drug complexes with the wild type DAT.

(2.44−3.05 Å) over all residues of protein was observed, variations came mostly from the EL2 domain of the protein (Figure S2A−E). Therefore, dDAT crystal structures did provide ideal templates to build homology models of DAT, especially for S1 site for drug binding.

Docking poses of six drugs in DAT's S1 binding site surrounded by TM 1, 3, 6, 8, and 10 are provided in Figure S3. To validate the drug−protein complexes constructed, cross-docking[45] was applied. In particular, cross-docking was carried out between dextroamphetamine and dextromethamphetamine, which were cocrystallized with dDAT in 4XP9 and 4XP6, respectively. As shown in Figure S4, the resulting cross-docking poses of both drugs were very similar in orientation and conformation comparing to their cocrystallized poses, which indicated the reliability of docking procedure used in this work. For those studied drugs, their resulting docking poses were selected based on a similar orientation as cocrystallized poses of their corresponding ligand templates. As shown in Figure S5, ammonium groups with protonated nitrogen ($-N^+$) of all studied drugs in DAT oriented in similar way as ligand templates in dDAT,[47,48,50] which formed an ionic interaction with Asp46 in dDAT (Asp79 in DAT). According to the overlay for dextroamphetamine, dextromethamphetamine, dexmethylphenidate, and R-bupropion with their templates (Figure S5A, B, D, and E), it was clear that aromatic groups of drugs embedded in hydrophobic cleft in similar conformational orientation as their cocrystallized ligand templates. The best docking pose of atomoxetine was also identified by its aromatic group and aryloxy inserting into two hydrophobic clefts in a similar way as S-nisoxetine (Figure S5C), and the selection of docking pose for R-modafinil should consider the conformation of sulfinyl group based on previous work[51] because of the same phenyl groups (Figure S5F).

Assessment of ADHD Drugs' Binding Modes in DAT. *Analysis of Simulation Stabilities and Binding Free Energy.* Six systems were assessed by 900 ns MD simulation, and the root-mean-square deviation (RMSD) was applied to assess whether the system reached the equilibration state or not. As illustrated in Figure S6, the RMSDs of protein backbone atoms, ligand heavy atoms, and binding site residue atoms are provided, and each system reached equilibration around 100 ns. In this study, simulation was extended by 50 ns to demonstrate the state of equilibration, and only slight fluctuation (within 1 Å) in monitored RMSD was observed in Figure S6.

Binding free energies (ΔG_{calc}) of six ADHD drugs in DAT were calculated and compared with the previous experiments[33,52−55] Experimental binding affinities (ΔG_{exp}) were estimated based on the K_i values.[25,61−64] As shown in Table 2, calculated binding affinities (ΔG_{calc}) were overestimated compared to the experimental ones. For drugs with similar structures and binding modes, entropy contribution could be omitted if only the relative order of binding affinities was of interest.[56] The relative difference of calculated binding energies ($\Delta\Delta G_{calc}$) and that of experimental ones ($\Delta\Delta G_{exp}$) among ADHD drugs were thus calculated (Table 2) to interpret whether the overestimation came from the exclusion of entropy or not. Moreover, Figure 1 further provided the chart of

DOI: 10.1021/acschemneuro.7b00173
ACS Chem. Neurosci. 2017, 8, 1416−1428

Table 3. Comparison of Binding Free Energies Calculated by the in Silico Mutation Analyses of This Study with That of Site-Directed Mutagenesis Experiments[40,51,63] and NET-like Mutational Experiments in DAT[65] (ΔG was in kcal/mol)[a]

ADHD drug	mutation site(s) (sensitivity profile)[b]	calculation results		reported experimental results	
		$\Delta\Delta G_{calc}$[c]	.FC_{calc}[d]	FC_{exp}[e]	$\Delta\Delta G_{exp}$[f]
comparison between the site-directed mutagenesis experiments[40,51,63] and the in silico single point mutation analyses					
dexmethylphenidate	W84L (NS)	−0.50	0.44	0.52 (0.38, 0.73)	−0.40 (−0.60, −0.19)
	D313N (NS)	−0.49	0.45	0.54 (0.44, 0.67)	−0.38 (−0.51, −0.25)
dextroamphetamine	W84L (MS)	0.47	2.15	2.51 (2.12, 2.95)	0.57 (0.46, 0.67)
	D313N (SE)	1.53	12.01	12.71 (10.74, 14.95)	1.56 (1.46, 1.66)
dextromethamphetamine	W84L (ME)	0.74	3.33	3.38 (2.53, 4.48)	0.75 (0.57, 0.92)
	D313N (ME)	0.74	3.33	4.27 (3.39, 5.41)	0.89 (0.75, 1.04)
R-bupropion	W84L (ME)	0.47	2.15	2.33 (2.13, 2.58)	0.52 (0.47, 0.58)
	D313N (NS)	−0.01	0.98	1.11 (0.98, 1.26)	0.06 (−0.01, 0.14)
R-modafinil	Y156F (SE)	1.64	14.36	14.40 (8.33, 22.39)	1.64 (1.30, 1.91)
comparison between the NET-like mutational experiments in DAT[65] and the in silico single point mutation analyses					
atomoxetine	S149A-F155Y-V318I-C319F-A423S-S429A	−0.75	0.30	0.55 (0.38−0.77)	−0.37 (−0.60, −0.16)
R-bupropion		−0.49	0.45	0.47 (0.32−0.67)	−0.46 (−0.70, −0.25)

[a]Detailed information of each energy term calculated can be found in Table S2. [b]Sensitivity profile of reported mutation sites.[40,51,63] SE, sensitive mutation ($FC_{exp} \geq 5$); MS, medium sensitive mutation ($2 \leq FC_{exp} < 5$); NS, nonsensitive mutation ($0.5 \leq FC_{exp} < 2$). [c]$\Delta\Delta G_{calc} = \Delta G_{mutation} - \Delta G_{wildtype}$. [d]Fold changes of potency measured by MD simulation (FC_{calc}) were derived from equation: $\Delta\Delta G_{calc} = RT\ln(FC_{calc})$, where R = 8.314J/(mol·K) and T = 310 K. [e]Fold changes of potency measured by reported experiments ($FC_{exp} = K_{i_{mutation}}/K_{i_{wildtype}}$).[40,51,63,65] Numbers in the brackets indicate the fold changes derived from the mean experimental values of both $K_{i_{mutation}}$ and $K_{i_{wildtype}}$ The first number in the brackets indicates the minimum fold changes, while the second one indicates the maximum fold changes. [f]$\Delta\Delta G_{exp}$ values were derived from the FC_{exp} by the equation $\Delta\Delta G_{exp} = RT\ln(FC_{exp})$, where R = 8.314J/(mol·K) and T = 310 K.

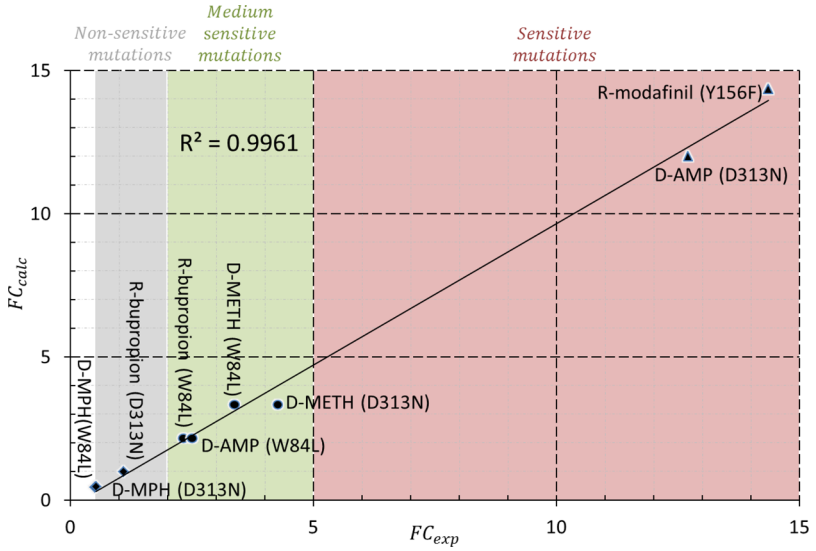

Figure 2. Graphical representation of correlation between the fold changes of simulation (FC_{calc}) and that of experiment (FC_{exp}) for nine studied point mutations in five drug−DAT complexes. The experimental fold change was measured by $FC_{exp} = K_i$ (mutation)/K_i (wild type), and the calculated one was derived from $\Delta\Delta G_{calc} = RT\ln(FC_{calc})$. Sensitivity profile of those nine point mutations were categorized into three groups: (1) sensitive mutation[64] ($FC_{exp} \geq 5$, pink color), (2) medium sensitive mutation[64] ($2 \leq FC_{exp} < 5$, light green), and (3) nonsensitive mutation[64] ($0.5 \leq FC_{exp} < 2$, gray color). The five drug−DAT complexes measured in this study included D-AMP (dextroamphetamine), D-METH (dextromethamphetamine), D-MPH (dexmethylphenidate), *R*-bupropion, and *R*-modafinil. Corresponding point mutations in these five complexes are provided in brackets.

correlation between $\Delta\Delta G_{calc}$ and $\Delta\Delta G_{exp}$, which correlated very well with each other (R^2 = 0.8976). The ascending trend of energy difference ($\Delta\Delta G_{exp}$) from experiment[25,61−64] was reproduced very well by $\Delta\Delta G_{calc}$ in this study, though their values were still estimated higher than experiment.[25,61−64] The overestimated energy calculated in this work was also found in other publication using the MM/GBSA methods.[57−62] In Table S1, the detailed contributions of each energy components in eq 1 are listed. As shown, the binding of ADHD drugs to DAT was mainly contributed by energy terms of van der Waals (ΔE_{vdW}) and electrostatic interaction (ΔE_{ele}), but hampered by that of polar solvent energy (ΔG_{pol}).

Validation of the Simulation Models. Besides the good correlation between simulation and experiment shown in previous section, three lines of evidence were further provided to validate simulation models constructed in this study. The first line of evidence was the capability of MD simulation in discovering the sensitivity profile of DAT residues revealed by mutagenesis experiments. Because the sensitivity profile could reveal the binding mode of ADHD drugs,[40,51,63] variations in

DOI: 10.1021/acschemneuro.7b00173
ACS Chem. Neurosci. 2017, 8, 1416−1428

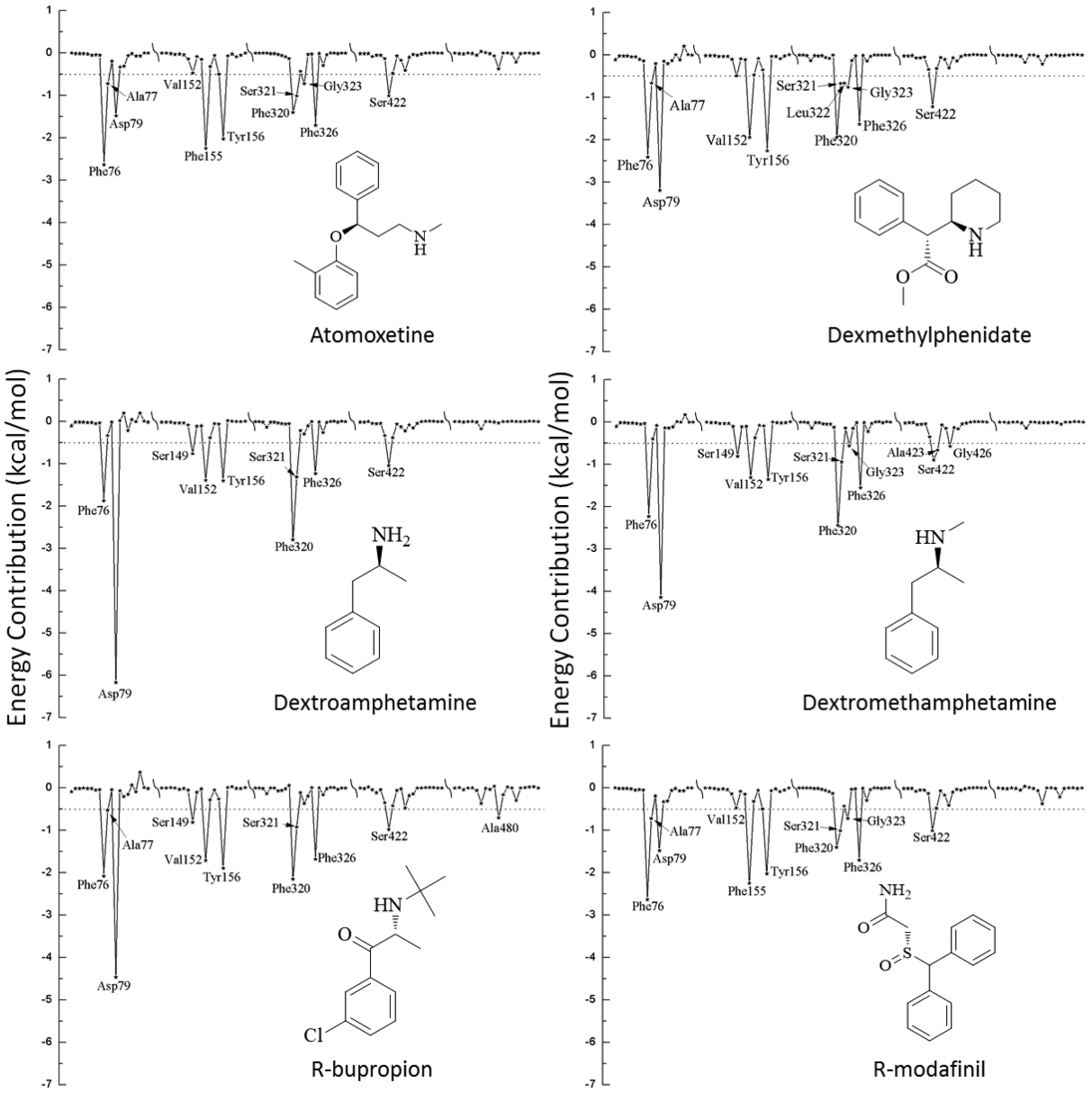

Figure 3. Per-residue binding free energy decomposition of six studied drug−DAT complexes. Residues with high energy contribution (the absolute energy contribution ≥ 0.5 kcal/mol) were labeled.

binding energies before and after in silico mutation were calculated. In this work, two sensitive mutations with ≥5-fold changes[64] in binding affinity (D313N[63] and Y156F[51] for binding of dextroamphetamine and *R*-modafinil, respectively), 4 medium sensitive ones with less than 5 but no less than 2-fold changes[64] (W84L[40,63] for dextroamphetamine, dextromethamphetamine, and *R*-bupropion and D313N[63] for binding of dextromethamphetamine) and three nonsensitive ones with less than 2-fold changes[64] (D313[40] for both dexmethylphenidate and *R*-bupropion and W84L[40] for dexmethylphenidate) identified by previous experimental mutagenesis studies[40,51,63] were selected and extensively explored. In particular, DAT of those mutations in complex with the corresponding ADHD drugs were studied by adding 20 ns simulation based on the MD-simulated wild type DAT. As shown in Figure S7, RMSD plots of ligand binding site backbone, ligand heavy atoms, and protein backbone for nine single-point mutant DATs complexed with studied drugs as a function of simulations time are provided. These plots monitored whether those simulations of mutant complexes reached equilibration within the additional 20 ns simulations. As shown in Figure S7, the simulation of all complexes reached equilibration around 15 ns, and the last 5 ns equilibrium trajectory was utilized to calculate the $\Delta\Delta G_{calc}$ in Table 3 and Table S2. The resulting binding energies and corresponding fold changes in drug affinity calculated by *in silico* mutations were demonstrated in Table 3, and contributions of each energy term were shown in Table S2. As shown, the sensitivity profile of DAT residues revealed by experiments[40,51,63] were completely reproduced by the simulation (FC_{calc}) of this study. In particular, two sensitive ($FC_{calc} > 12.01$), four medium sensitive ($2.15 \leq FC_{calc} \leq 3.33$), and three nonsensitive ($0.44 \leq FC_{calc} \leq 0.98$) mutations were discovered. Moreover, correlation between the fold changes of simulation (FC_{calc}) and that of experiment (FC_{exp}) for those nine point mutations is further illustrated in Figure 2, which resulted in a good correlation ($R^2 = 0.9961$). In sum, simulation

DOI: 10.1021/acschemneuro.7b00173
ACS Chem. Neurosci. 2017, 8, 1416−1428

models constructed in this study were capable of discovering sensitivity profile of DAT residues revealed by experiments, which could be considered as suitable evidence to verify the constructed models. Moreover, examples of variation in ligand binding site backbone, ligand heavy atoms and protein backbone among different mutants with drugs docked were depicted by the average RMSD (±SD) from the last 5 ns equilibrium trajectories (Figure S8). The average RMSD of ligand binding site backbone for dexmethylphenidate bound DAT caused by W84L was lower than that by D313N, indicating a relatively weaker influence on the conformation change of the binding site induced by W84L than that of D313N (in Figure S8A). Meanwhile, W84L and D313N led to similar degree of conformation changes in the binding sites with dextroamphetamine, dextromethamphetamine and *R*-bupropion bound. Conformation changes in DAT binding pocket and shifts of drugs into the pocket are also shown in Figure S9. Although the above sensitive or medium sensitive mutation D313N reported by a previous study[63] was located outside the S1 pocket, MD simulation was capable of identifying its sensitivity profile. As demonstrated in Figure S9, D313N indirectly but significantly influenced DAT's interaction with dextroamphetamine by inducing dramatic conformation change of residues Phe320 and Ser422. Similar to dextroamphetamine, D313N indirectly affected dextromethamphetamine's binding, and significant conformation changes in Tyr156 and Gly426 were observed (Figure S9).

The second line of evidence was from a recently identified group of residues that collectively control drug selectivity to NET.[65] Specifically, the mutations on six residues (Ser149, Phe155, Val318, Cys319, Ala423 and Ser429) in the S1 site of DAT to the complementary residues in NET transferred NET-like pharmacology to DAT.[65] However, the selectivity of two ADHD drugs (atomoxetine and R-bupropion) to NET was tested to be not sensitively determined by those 6 residues, and it was noteworthy that the S1 site of DAT has little effect on ADHD drugs' selectivity.[65] In this work, in silico mutations on these 6 residues to their corresponding residues in NET (S149A-F155Y-V318I-C319F-A423S-S429A) were explored. As illustrated in Figure S10, atomoxetine and *R*-bupropion in complex with the NET-like DAT were simulated by extending 20 ns simulation based on the MD-simulated wild type DAT. The resulting binding free energies and corresponding fold changes in affinity calculated by in silico mutational analyses were shown in Table 3, and the contributions of each energy term were demonstrated in Table S2. As shown, the nonsensitive determination of the drugs' selectivity by those six residues[65] was reproduced by simulation (FC_{calc}). In particular, values of FC_{calc} equaled to 0.30 and 0.45 for atomoxetine and *R*-bupropion, respectively, which were comparable to that of experiment.[65] Since those additional 20 ns simulations were all based on the models of wild type DAT constructed in this study, this reproduction of experiments could act as another line of evidence for verifying our resulting simulation models. The conformational changes in DAT's S1 pocket and orientation shifts of atomoxetine and *R*-bupropion to accommodate into the pocket were illustrated in Figure S11.

The above evidence was further supported by the third line of evidence from the crystallography study, which reported cocrystallized structures of amphetamine and methamphetamine in dDAT.[47] Of these two drug−dDAT complexes, the amino group of both ADHD drugs interacted with dDAT's Asp46 residue (the corresponding residue Asp79 in DAT), and occupied the cavity formed by residues Phe43, Ala44, Phe319, and Ser320 in dDAT (the corresponding residues Phe76, Ala77, Phe320, and Ser321 in DAT).[47] Furthermore, the phenyl group of both drugs were stabilized by inserting into hydropholic cleft formed by Val120, Tyr124, Phe319, Phe325, and Ser422 in dDAT (the corresponding residues Val152, Tyr156, Phe320, Phe326, and Ala423 in DAT), which further stabilized amphetamine and methamphetamine in the S1 site of DAT.[47] In this work, all of those mentioned residues were identified as high contribution ones (with the absolute energy contribution ≥ 0.5 kcal/mol) for the binding of ADHD drugs (shown in Figure 3), which could be the third evidence for verifying our resulting simulation models.

Binding Modes of ADHD Drugs in DAT. Representative interaction snapshots of studied complexes extracted from equilibrated MD trajectories were shown in Figure S12. All structures demonstrated electrostatic interactions between protonated nitrogen ($-N^+$) in the ammonium group of ADHD drugs and negative charged oxygen (O−) of Asp79, and the electrostatic interaction including salt bridge and hydrogen bond (Figure S13 and Table S3) were relatively stable during the MD simulation. These were consistent with previous studies that the interaction between ADHD drugs' ammonium group and Asp79 was essential for their recognition.

As illustrated by the binding free energy decomposition of DAT's residues (Figure 3), 11, 11, 9, 12, 11, and 11 residues contributed significantly (absolute energy contribution ≥ 0.5 kcal/mol) to binding of atomoxetine, dexmethylphenidate, dextroamphetamine, dextromethamphetamine, *R*-bupropion, and *R*-modafinil, respectively. Among those residues above, Phe326 was identified as distinguished one in discriminating energy contributions between psychostimulants (−1.23 to −1.63 kcal/mol) and inhibitors with little abuse liability (−1.68 to −1.75 kcal/mol). As reported, differences between binding modes of approved psychostimulants and that of inhibitors with little abuse liability could facilitate the discovery of mechanism underlying ADHD drugs' addictiveness.[66] To the best of our knowledge, Phe326 was the first reported residue able to discriminate the addictiveness of ADHD drugs. However, to fully understand the way how different drug structures affected their abuse liability, collective impacts of residues (not just Phe326) discriminating drugs' addictiveness should be further identified and assessed. Thus, differences in molecular modes of interaction between psychostimulants (amphetamine, methamphetamine, and methylphenidate) and drugs of little addictiveness (atomoxetine, bupropion and modafinil) were further explored from perspective of per-residue energy contribution to the drugs' binding.

Comparing the Binding Modes of Addictive ADHD Drugs and that of Nonaddictive Ones. To differentiate the binding modes between two types of ADHD drugs (addictive and nonaddictive), the hierarchical clustering was applied to identify the binding modes of each drug type. In particular, 224 (for addictive type) and 246 (for nonaddictive type) residues with energy contribution (≠0 kcal/mol) to at least one drug in their corresponding drug type were clustered based on their per-residue binding energies. As illustrated by the hierarchical trees in Figures S14 and S15, five residue groups (A−E) were discovered for both addictive and nonaddictive ADHD drugs. Per-residue binding free energies favoring the drugs' binding were colored in red, with the highest energy (−6.17 and −4.46 kcal/mol for addictive and nonaddictive drugs, respectively) set

DOI: 10.1021/acschemneuro.7b00173
ACS Chem. Neurosci. 2017, 8, 1416−1428

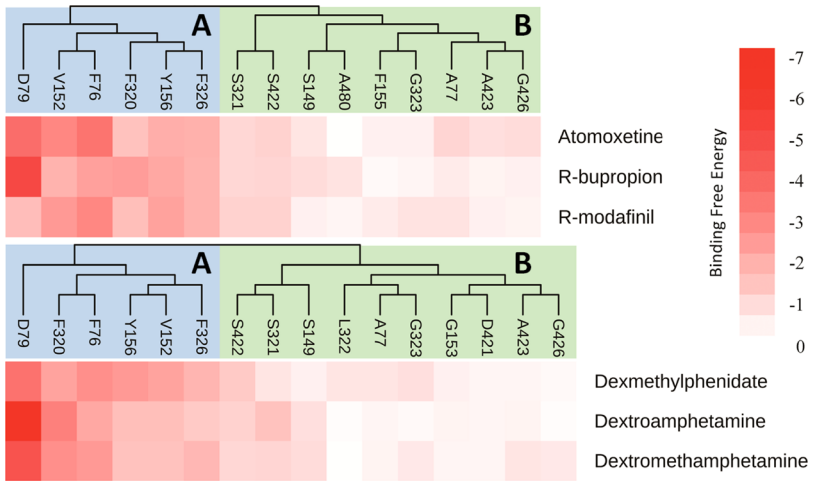

Figure 4. Comparison of the residues in group A (light blue background) and B (light green background) identified in Figures S14 and S15. Per-residue binding energy contributions favoring ligand binding are displayed in red, with the highest contribution set as exact red and lower contributions gradually fading toward white (no contribution).

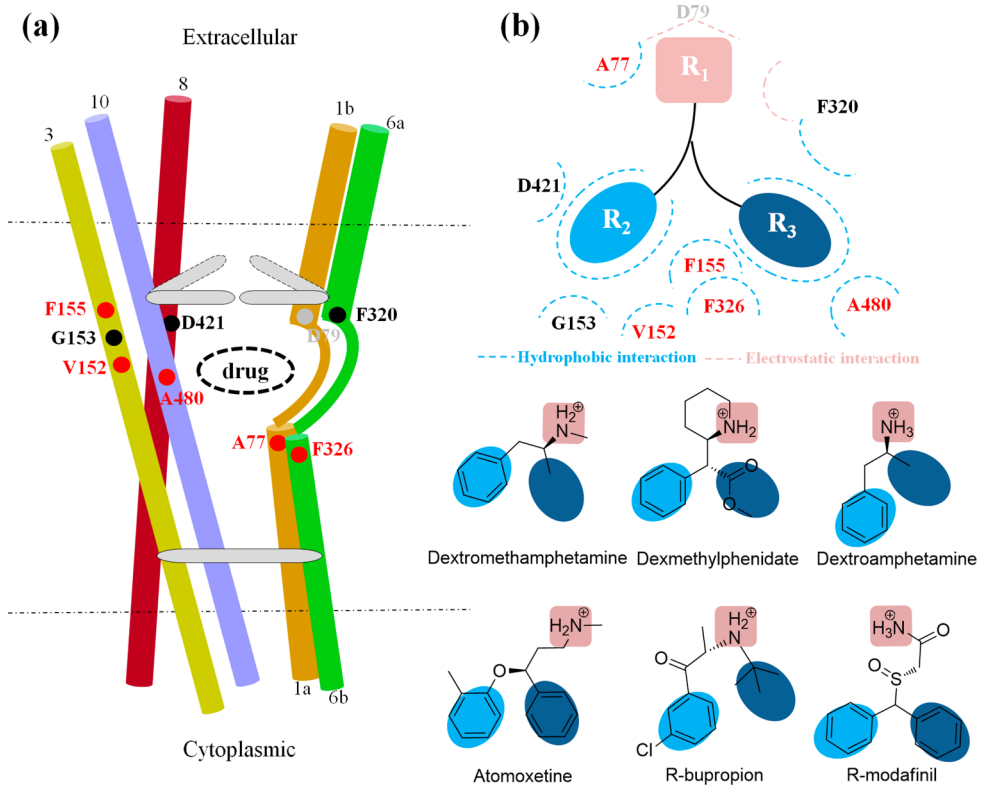

Figure 5. Binding mode of studied ADHD drugs in DAT. (a) Side view of drug binding site surrounded by eight residues of significant energy fold changes between addictive and nonaddictive drugs. Residues preferentially binding nonaddictive drugs were represented in red, while residues favoring binding of addictive drugs were shown in black. (b) Schematic representation of the binding modes between drugs and residues. Binding mode of studied drugs was collectively defined by electrostatic and hydrophobic interactions between three chemical groups (R_1, R_2, and R_3) and eight residues colored in the same way as (a). R_1 (reddish) were ammonium group with electrostatic interaction to residues in the vicinity, especially the D79. R_2 (light blue) and R_3 (dark blue) were aromatic moieties with only hydrophobic interaction to nearby residues.

as exact red and lower energies gradually fading toward white (0 kcal/mol). Per-residue energies hampering the drugs' binding are displayed in blue, with the highest (0.21 and 0.37 kcal/mol for addictive and nonaddictive drugs, respectively) set as exact blue and lower ones gradually fading toward white. To avoid any misunderstanding, energies represented by exact red are 29 and 12 times stronger than that by exact blue in Figures S14 and S15, respectively.

The per-residue energies of residue groups A and B were consistently higher for all drugs in each type than those of groups C−E, which made them the primary contributors favoring the drugs' binding. Therefore, those residues in group A and B were further selected to comparatively analyze the binding modes of addictive and nonaddictive drugs (Figure 4). As shown, six residues (Phe76, Asp79, Val152, Tyr156, Phe320, and Phe326) in group A were the major contributors for the

DOI: 10.1021/acschemneuro.7b00173
ACS Chem. Neurosci. 2017, 8, 1416−1428

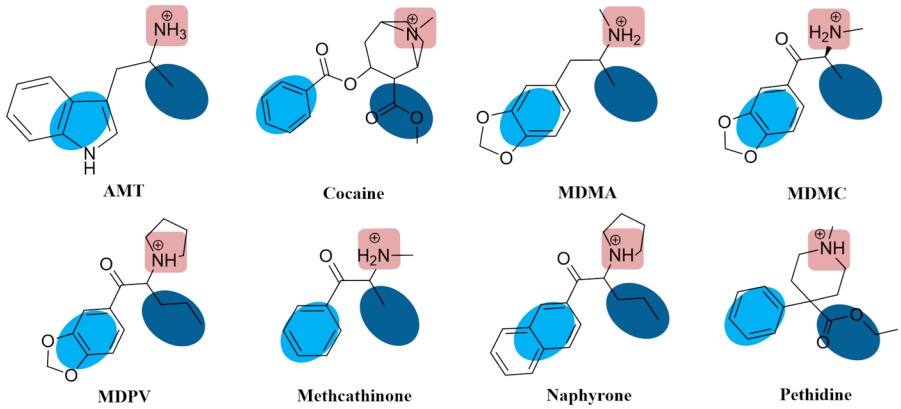

Figure 6. Structures and functional groups of eight controlled substances with high affinity to DAT (IC_{50}/K_i < 1 μM) scheduled by the United States Controlled Substances Act collected from official Web site of the United States Electronic Code of Federal Regulations (ECFR). Functional groups (R_1, R_2, and R_3) of those eight substances were identified by molecular docking, and are marked by reddish solid rectangular (R_1), light blue (R_2), and dark blue (R_3) solid ellipse. Detailed information can also be found in Table S5.

binding of both drug types, which consisted of 57.73−67.59% and 52.32−62.39% of the total binding energy for addictive and nonaddictive drugs, respectively. Moreover, there were 9 and 10 residues identified as very important contributors for the binding of addictive and nonaddictive drugs (group B), which offered 23.90−26.33% and 24.30−25.93% of the total binding energy for each drug type. Among those important residues, seven residues (Ala77, Ser149, Ser321, Gly323, Ser422, Ala423, and Gly426) were shared by both types, while three (Gly153, Leu322, and Asp421) and two (Phe155 and Ala480) residues were distinct for addictive and nonaddictive drugs, respectively. Conformations of 6 studied drugs accommodating into those 18 residues were illustrated in Figure S16. Due to the primary energy contribution (>75%) offered by those 18 residues for both drug types, a comparatively analysis on energies of those residues between addictive and nonaddictive drugs could offer great insight into the understanding of how different drug structures affected their abuse liability.

Identifying Functional Groups of Studied ADHD Drugs Discriminating their Addictive Profile. To understand how different drug structures discriminating the addictive profile of the studied drugs, the binding free energies of 18 residues shown in Figure 4 were statistically compared by fold change analysis. As demonstrated in Table S4, eight residues (Ala77, Val152, Gly153, Phe155, Phe320, Phe326, Asp421, and Ala480) of significant fold changes (>1)[67] between addictive and nonaddictive ADHD drugs were identified. Five out of those eight residues (Ala77, Val152, Phe155, Phe326, and Ala480) preferentially binding nonaddictive drugs are shown in red, while the remaining three (Gly153, Phe320, and Asp421) favoring addictive ones are shown in black (Figure 5a). Based on the conformation of six studied drugs surrounded by eight residues (Figures 5a and S17), a schematic representation of the binding modes between drugs and residues are generalized and illustrated in Figure 5b, which was collectively defined by electrostatic and hydrophobic interactions between three chemical groups (R_1, R_2, and R_3) and those eight residues identified above. In particular, the R_3 occupied the hydrophobic cleft sculpted by Phe155, Phe326, and Ala480. Significant reduction in hydrophobic interaction of addictive drugs induced by these 3 residues was identified and reflected by lower hydrophobic property in R_3 of addictive drugs (methyl and methoxycarbonyl groups) than that of nonaddictive ones (phenyl and trimethyl groups). Similarly, the hydrophobic interactions of R_2 in addictive drugs were substantially reduced, which was contributed by two hydrophilic (Gly153 and Asp421) and three hydrophobic (Val152, Phe155, and Phe326) residues. This reduction should come from weaker hydrophobic property in R_2 of addictive drugs (phenyl group) than that of nonaddictive ones (chlorine- and methyl-substituted phenyl groups). Structural variation in studied drugs could also induce changes in interaction between R_1 and surrounding residues (Ala77 and Phe320).

The identified reductions of hydrophobic property in both R_2 and R_3 of studied addictive drugs could be further observed in eight controlled substances inhibiting DAT (IC_{50}/K_i < 1 μM) scheduled by the United States Controlled Substances Act[25] (Table S5). These eight substances were collected from the official Web site of the United States Electronic Code of Federal Regulations (http://www.ecfr.gov) including six schedule I (AMT, MDMA, MDMC, MDPV, methcathinone, and naphyrone) and two schedule II (cocaine and pethidine) controlled substances. As shown in Figure 6, hydrophobic property in R_3 of all 8 controlled substances (methyl, propyl, methoxycarbonyl and ethoxycarbonyl groups) was weaker than that of nonaddictive ADHD drugs studied (phenyl and trimethyl groups). Similarly, the hydrophobic property in R_2 of those 8 substances (3,4-methylenedioxyphenyl, indolyl, naphthalene and phenyl group) was generally lower than that of studied nonaddictive drugs (chlorine- and methyl-substituted phenyl groups). In summary, the reduction of hydrophobic property in 2 functional groups of those 8 reported controlled substances agreed well with the finding of this work. Increased hydrophobicity of substituted-group in R_2 and R_3 could lead to the reduction of ADHD drugs' addictiveness by enhanced hydrophobic interactions with DAT. This could facilitate the discovery of improved ADHD drugs with reduced addictive profile.

CONCLUSIONS

In this work, a comparative analysis on the molecular mode of interaction discriminating addictiveness among six ADHD drugs was carried out by multiple computational methods. As a result, eight key residues of significant fold change in binding energy and the hydrophobic property of two key functional groups in studied drugs discriminating addictiveness were discovered. The identified variations in molecular mode of

DOI: 10.1021/acschemneuro.7b00173
ACS Chem. Neurosci. 2017, 8, 1416−1428

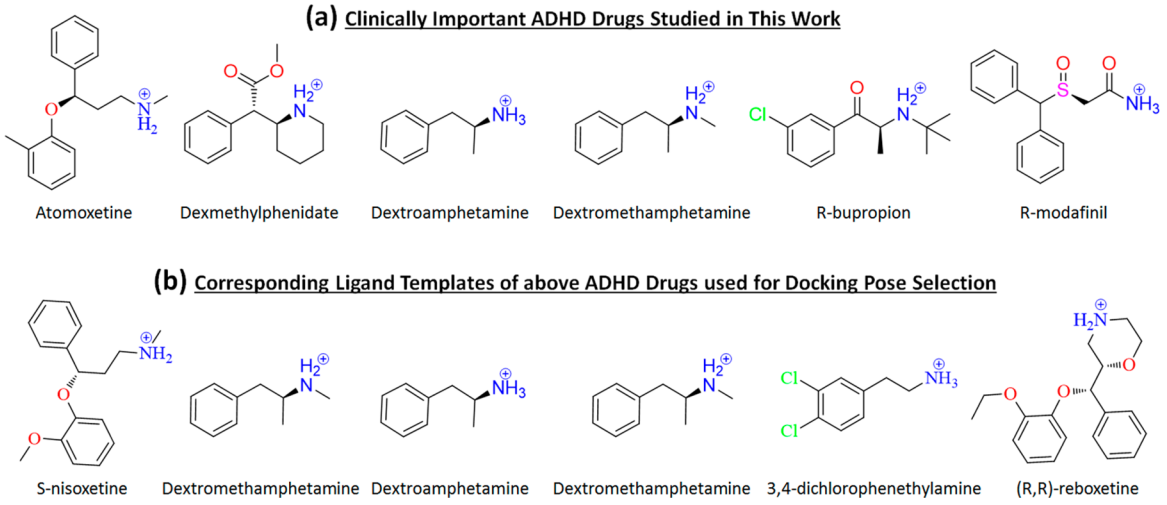

Figure 7. Structures of (a) six clinically important ADHD drugs studied in this work and (b) their corresponding ligand templates used for docking pose selection.

interaction indicated increased hydrophobicity of substituted-group in R_2 and R_3 could lead to the reduction of ADHD drugs' addictiveness by enhanced hydrophobic interactions with DAT, which shed light on the mechanism underlining the addictiveness of studied drugs. This result may therefore be utilized as structural and energetic blueprint for discovering improved ADHD therapeutics.

METHODS

Collection of ADHD Drugs. Among those drugs listed in Table 1, nine were reported as active in inhibiting DAT (<10 μM). Five out of these nine were racemic compounds (amphetamine, bupropion, methamphetamine, methylphenidate, and modafinil), and D-enantiomers of amphetamine and methylphenidate had already been approved. In the meantime, the D-enantiomer of methamphetamine was reported to offer the main therapeutic efficacy,[68] and *R*-bupropion and *R*-modafinil demonstrated greater efficacy in inhibiting DAT.[40,69] Thus, six drugs of distinct structure (atomoxetine, dexmethylphenidate, dextroamphetamine, dextromethamphetamine, *R*-bupropion, and *R*-modafinil) in Figure 7a were simulated in this study, including three psychostimulants and three drugs of little addictiveness. It was necessary to clarify that lisdexamfetamine was an inactive prodrug of dextroamphetamine,[70] and no simulation was thus applied.

Homology Modeling. Sequences alignment between DAT and *Drosophila melanogaster* dopamine transporter (dDAT) using ClustalW2[71] in Figure S18 showed their higher sequence identity with more than 55%. Therefore, crystal structures of dDAT complexed with various ligands[47,48] were used to construct homology models of DAT by automated mode in SWISS-MODEL.[72] Particularly, ligands structurally similar by visual inspection to any of the studied ADHD drugs were identified (Figure 7b) and the corresponding dDAT structures were selected as templates for homology modeling (Table S6). Comparing to the popular template LeuT,[73] dDAT showed much higher sequence identity (55.2−56.5%) with DAT, which made it reliable starting point for simulation. Sequences in model construction covered all DAT's transmembranes (TMs) and loops, and stereochemical quality were validated by the PROCHECK.[74,75] Additionally, two functional Na^+ and one Cl^- were fitted into binding sites of all models via PyMOL.[76] Two cholesterols were added into models from 4XNU, 4XPH, and 4XNX, while cholesterol and cholesteryl hemisuccinate were transferred into models from 4XP6 and 4XP9.

Molecular Docking. Initial poses for simulation were identified by molecular docking via standard precision (SP) in Schrödinger Glide module.[77] In particular, by using Receptor Grid Generation tool in Glide,[77] the docking grid box for each studied drug was defined by centering on the corresponding ligand template in modeled DAT S1 binding site (surrounded by TM 1, 3, 6, 8, and 10).[47,48] As a results, the docking poses of six studied drugs with the most similar orientation with those of ligand templates (Table S6) were selected as their initial binding poses for simulation. To validate the reliability of molecular docking procedure in this study, cross-docking[78] was applied. Detailed information on molecular docking and cross-docking is extensively described in Supporting Information Methods.

Protein−Ligand/Membrane System Setup and MD Simulation. Protein−ligand/membrane systems were constructed by inserting the resulting docking complexes into a 1-palmitoyl-2-oleoylphosphatidylcholine (POPC) bilayer generated by the Membrane Builder in CHARMM-GUI.[79] These systems were solvated with TIP3P water of 20 Å thickness[80] and neutralized Na^+ and Cl^- at salt concentration of 0.15 mol/L. Each system contained 92 000−99 000 atoms per periodic cell with various box size as summarized in Table S6. Detailed information on the above process is extensively described in Supporting Information Methods.

MD simulations were carried out using AMBER14 package[81] based on ff14SB and Lipid14 force fields for proteins and lipids respectively by GPU-accelerated PMEMD.[45] Prior to each simulation, systems underwent a succession of pretreatments including (1) steepest descent minimization, (2) heating to 310 K through two sequential stages, and (3) 5 ns equilibration at 310 K.[45,82] After these, 150 ns MD simulation was executed at 310 K and 1 atm in NPT ensemble by the periodic boundary condition. Moreover, the long-range electrostatic interaction (cutoff = 10 Å) was used to evaluate direct space interaction with the particle-mesh Ewald method,[83] and all bonds involving hydrogen atoms were constrained by using the SHAKE algorithm[84] with a 2 fs time step. Finally, 500 snapshots were retrieved from the last 50 ns equilibrium trajectory of each system. Detailed information can be found in Supporting Information Methods.

Binding Free Energy Analysis. Total binding free energies (ΔG_{calc}) neglected entropic contribution were calculated by MM/GBSA method according to 500 snapshots of each single-trajectory.[85−88] For each snapshot, the binding energy was obtained by the following equation:

$$\Delta G_{calc} = \Delta E_{vdW} + \Delta E_{ele} + \Delta G_{pol} + \Delta G_{nonpol} \quad (1)$$

ΔE_{vdW} and ΔE_{ele} originate from van der Waals interaction and electrostatic contribution in gas phase, respectively. ΔG_{pol} and ΔG_{nonpol} indicate polar and nonpolar solvent interaction energies. In particular, ΔG_{nonpol} was calculated by 0.0072 × ΔSASA, and ΔSASA was estimated by linear combination of pairwise overlaps method (LCPO) with 1.4 Å Probe radii.[89,90] Moreover, per-residue decomposition energy ($\Delta G_{calc}^{per-residue}$) used to quantitatively evaluate each residue's contribution to the binding was calculated by the following equation:

DOI: 10.1021/acschemneuro.7b00173
ACS Chem. Neurosci. 2017, 8, 1416−1428

$$\Delta G_{calc}^{per-residue} = \Delta E_{vdW}^{per-residue} + \Delta E_{ele}^{per-residue} + \Delta G_{pol}^{per-residue} + \Delta G_{nonpol}^{per-residue} \quad (2)$$

$\Delta E_{vdW}^{per-residue}$, $\Delta E_{ele}^{per-residue}$, and $\Delta G_{pol}^{per-residue}$ were the same as those in eq 1, and nonpolar solvation free energy contribution was estimated as $\Delta G_{nonpol}^{per-residue} = 0.0072 \times \Delta SASA$. The ΔSASA was achieved by using the icosahedron (ICOSA) method.[81]

Hierarchical Clustering Analysis on Per-residue Binding Free Energies. Here, 224 residues with contributions to the binding of at least one psychostimulant (≠ 0 kcal/mol) were identified, and corresponding per-reside energies to 3 studied psychostimulants were used to generate 3-dimensional vectors. Similarly, 246 residues for 3 little addictive drugs were identified. Then, 224 and 246 vectors were analyzed by the hierarchical clustering algorithm in the *R* Statistic analysis software,[91] respectively. Similarity degrees among vectors (residues) were reflected by the Manhattan distance:

$$\text{distance}(a, b) = \sum_{i=1}^{l} |a_i - b_i| \quad (3)$$

where *l* indicates the dimension of vector and *i* refers to certain residue energy for each ADHD drug. The Ward's minimum variance was used to minimize the total within-cluster variance.[92] The hierarchical trees were visualized by using the online tool iTOL.[93]

■ ASSOCIATED CONTENT

Supporting Information

The Supporting Information is available free of charge on the ACS Publications website at DOI: 10.1021/acschemneuro.7b00173.

Decriptions of methods applied in this study; comparison of calculated and experimental binding energies of drug; energy terms calculated in mutation analysis; hydrogen bond analysis; per-residue contributions of key residues' energy; data of controlled substances; data of homology modeling and protein−ligand/membrane system; Ramachandran plots of homology models; comparison of homology models constructed by different templates; docking poses of studied drugs; cross-docking; selection of drugs' initial conformation; RMSD of the MD simulation; conformation comparison of the mutation analysis; representative snapshot of drug-target interaction; distance of the salt bridge interaction; clustering trees based on per-residue energy; conformation of drug-target interaction with important residues highlighted; sequence alignment between DAT and dDAT (PDF)

■ AUTHOR INFORMATION

Corresponding Authors

*Mailing address: College of Pharmaceutical Sciences, Zhejiang University, Hangzhou, China. E-mail: zhufeng.ns@gmail.com and zhufeng@cqu.edu.cn. Phone: +86-(0)23-65678468.

*Mailing address: School of Pharmaceutical Sciences, Chongqing University, Chongqing, China. E-mail: xueww@cqu.edu.cn. Phone: +86-(0)23-65678468.

ORCID

Weiwei Xue: 0000-0002-3285-0574

Feng Zhu: 0000-0001-8069-0053

Author Contributions

F.Z. and W.X. designed research. P.W., X.Z., T.F., and F.Z. performed research. P.W., X.Z., T.F., S.L., B.L., W.X., T.H., X.Y., and Y.C. analyzed the data. P.W., W.X., and F.Z. wrote the manuscript. All authors reviewed the manuscript.

Funding

This work was funded by the National Natural Science Foundation of China (21505009); the Precision Medicine Project of the National Key Research and Development Plan of China (2016YFC0902200); Innovation Project on Industrial Generic Key Technologies of Chongqing (cstc2015zdcy-ztzx120003); and Fundamental Research Funds for Central Universities (10611CDJXZ238826, CDJZR14468801, CDJKXB14011).

Notes

The authors declare no competing financial interest.

■ ABBREVIATIONS

ADHD, attention-deficit/hyperactivity disorder; NE, norepinephrine; DA, dopamine; sNRI, selective NE reuptake inhibitor; NET, norepinephrine transporter; DAT, dopamine transporter; MD, molecular dynamics; dDAT, *Drosophila melanogaster* dopamine transporter; hSERT, human serotonin transporter

■ REFERENCES

(1) Global Burden of Disease Study Collaborators (2015) Global, regional, and national incidence, prevalence, and years lived with disability for 301 acute and chronic diseases and injuries in 188 countries, 1990−2013: a systematic analysis for the global burden of disease study 2013. *Lancet 386*, 743−800.

(2) Franke, B., Vasquez, A. A., Johansson, S., Hoogman, M., Romanos, J., Boreatti-Hummer, A., Heine, M., Jacob, C. P., Lesch, K. P., Casas, M., Ribases, M., Bosch, R., Sanchez-Mora, C., Gomez-Barros, N., Fernandez-Castillo, N., Bayes, M., Halmoy, A., Halleland, H., Landaas, E. T., Fasmer, O. B., Knappskog, P. M., Heister, A. J., Kiemeney, L. A., Kooij, J. J., Boonstra, A. M., Kan, C. C., Asherson, P., Faraone, S. V., Buitelaar, J. K., Haavik, J., Cormand, B., Ramos-Quiroga, J. A., and Reif, A. (2010) Multicenter analysis of the SLC6A3/DAT1 VNTR haplotype in persistent ADHD suggests differential involvement of the gene in childhood and persistent ADHD. *Neuropsychopharmacology 35*, 656−64.

(3) Garcia Murillo, L., Ramos-Olazagasti, M. A., Mannuzza, S., Castellanos, F. X., and Klein, R. G. (2016) Childhood attention-deficit/hyperactivity disorder and homelessness: A 33-year follow-up study. *J. Am. Acad. Child. Adolesc. Psychiatry 55*, 931−936.

(4) Maia, T. V., and Frank, M. J. (2011) From reinforcement learning models to psychiatric and neurological disorders. *Nat. Neurosci. 14*, 154−62.

(5) Drerup, J. M., Hayashi, K., Cui, H., Mettlach, G. L., Long, M. A., Marvin, M., Sun, X., Goldberg, M. S., Lutter, M., and Bibb, J. A. (2010) Attention-deficit/hyperactivity phenotype in mice lacking the cyclin-dependent kinase 5 cofactor p35. *Biol. Psychiatry 68*, 1163−71.

(6) Brozoski, T. J., Brown, R. M., Rosvold, H. E., and Goldman, P. S. (1979) Cognitive deficit caused by regional depletion of dopamine in prefrontal cortex of rhesus monkey. *Science 205*, 929−32.

(7) Arnsten, A. F., and Li, B. M. (2005) Neurobiology of executive functions: catecholamine influences on prefrontal cortical functions. *Biol. Psychiatry 57*, 1377−84.

(8) Li, B., Tang, J., Yang, Q., Li, S., Cui, X., Li, Y., Chen, Y., Xue, W., Li, X., and Zhu, F. (2017) NOREVA: normalization and evaluation of MS-based metabolomics data. *Nucleic Acids Res.*, DOI: 10.1093/nar/gkx449.

(9) Castellanos, F. X., and Tannock, R. (2002) Neuroscience of attention-deficit/hyperactivity disorder: the search for endophenotypes. *Nat. Rev. Neurosci. 3*, 617−28.

(10) Yang, H., Qin, C., Li, Y. H., Tao, L., Zhou, J., Yu, C. Y., Xu, F., Chen, Z., Zhu, F., and Chen, Y. Z. (2016) Therapeutic target database update 2016: enriched resource for bench to clinical drug target and targeted pathway information. *Nucleic Acids Res. 44*, D1069−74.

(11) Zhu, F., Ma, X. H., Qin, C., Tao, L., Liu, X., Shi, Z., Zhang, C. L., Tan, C. Y., Chen, Y. Z., and Jiang, Y. Y. (2012) Drug discovery

DOI: 10.1021/acschemneuro.7b00173
ACS Chem. Neurosci. 2017, 8, 1416−1428

prospect from untapped species: indications from approved natural product drugs. *PLoS One 7*, e39782.
(12) Loo, S. K., Bilder, R. M., Cho, A. L., Sturm, A., Cowen, J., Walshaw, P., Levitt, J., Del'Homme, M., Piacentini, J., McGough, J. J., and McCracken, J. T. (2016) Effects of d-Methylphenidate, Guanfacine, and their combination on electroencephalogram resting state spectral power in attention-deficit/hyperactivity disorder. *J. Am. Acad. Child. Adolesc. Psychiatry 55*, 674−682.
(13) Zhu, F., Qin, C., Tao, L., Liu, X., Shi, Z., Ma, X., Jia, J., Tan, Y., Cui, C., Lin, J., Tan, C., Jiang, Y., and Chen, Y. (2011) Clustered patterns of species origins of nature-derived drugs and clues for future bioprospecting. *Proc. Natl. Acad. Sci. U. S. A. 108*, 12943−8.
(14) Zhu, F., Han, L., Zheng, C., Xie, B., Tammi, M. T., Yang, S., Wei, Y., and Chen, Y. (2009) What are next generation innovative therapeutic targets? Clues from genetic, structural, physicochemical, and systems profiles of successful targets. *J. Pharmacol. Exp. Ther. 330*, 304−15.
(15) Freyberg, Z., Sonders, M. S., Aguilar, J. I., Hiranita, T., Karam, C. S., Flores, J., Pizzo, A. B., Zhang, Y., Farino, Z. J., Chen, A., Martin, C. A., Kopajtic, T. A., Fei, H., Hu, G., Lin, Y. Y., Mosharov, E. V., McCabe, B. D., Freyberg, R., Wimalasena, K., Hsin, L. W., Sames, D., Krantz, D. E., Katz, J. L., Sulzer, D., and Javitch, J. A. (2016) Mechanisms of amphetamine action illuminated through optical monitoring of dopamine synaptic vesicles in Drosophila brain. *Nat. Commun. 7*, 10652.
(16) Cheng, J., Xiong, Z., Duffney, L. J., Wei, J., Liu, A., Liu, S., Chen, G. J., and Yan, Z. (2014) Methylphenidate exerts dose-dependent effects on glutamate receptors and behaviors. *Biol. Psychiatry 76*, 953−62.
(17) Zhu, F., Shi, Z., Qin, C., Tao, L., Liu, X., Xu, F., Zhang, L., Song, Y., Liu, X., Zhang, J., Han, B., Zhang, P., and Chen, Y. (2012) Therapeutic target database update 2012: a resource for facilitating target-oriented drug discovery. *Nucleic Acids Res. 40*, D1128−36.
(18) Madras, B. K., Miller, G. M., and Fischman, A. J. (2005) The dopamine transporter and attention-deficit/hyperactivity disorder. *Biol. Psychiatry 57*, 1397−409.
(19) Zhu, F., Han, B., Kumar, P., Liu, X., Ma, X., Wei, X., Huang, L., Guo, Y., Han, L., Zheng, C., and Chen, Y. (2010) Update of TTD: therapeutic target database. *Nucleic Acids Res. 38*, D787−91.
(20) Spencer, T., Biederman, J., Wilens, T., Doyle, R., Surman, C., Prince, J., Mick, E., Aleardi, M., Herzig, K., and Faraone, S. (2005) A large, double-blind, randomized clinical trial of methylphenidate in the treatment of adults with attention-deficit/hyperactivity disorder. *Biol. Psychiatry 57*, 456−63.
(21) Humphreys, K. L., Eng, T., and Lee, S. S. (2013) Stimulant medication and substance use outcomes: a meta-analysis. *JAMA. Psychiatry 70*, 740−9.
(22) Berman, S. M., Kuczenski, R., McCracken, J. T., and London, E. D. (2009) Potential adverse effects of amphetamine treatment on brain and behavior: a review. *Mol. Psychiatry 14*, 123−42.
(23) Dance, A. (2016) Smart drugs: A dose of intelligence. *Nature 531*, S2−3.
(24) Zhu, F., Zheng, C. J., Han, L. Y., Xie, B., Jia, J., Liu, X., Tammi, M. T., Yang, S. Y., Wei, Y. Q., and Chen, Y. Z. (2008) Trends in the exploration of anticancer targets and strategies in enhancing the efficacy of drug targeting. *Curr. Mol. Pharmacol. 1*, 213−32.
(25) Molina, B. S., Hinshaw, S. P., Eugene Arnold, L., Swanson, J. M., Pelham, W. E., Hechtman, L., Hoza, B., Epstein, J. N., Wigal, T., Abikoff, H. B., Greenhill, L. L., Jensen, P. S., Wells, K. C., Vitiello, B., Gibbons, R. D., Howard, A., Houck, P. R., Hur, K., Lu, B., and Marcus, S. (2013) Adolescent substance use in the multimodal treatment study of attention-deficit/hyperactivity disorder (ADHD) (MTA) as a function of childhood ADHD, random assignment to childhood treatments, and subsequent medication. *J. Am. Acad. Child. Adolesc. Psychiatry 52*, 250−63.
(26) Volkow, N. D., Fowler, J. S., Wang, G. J., Baler, R., and Telang, F. (2009) Imaging dopamine's role in drug abuse and addiction. *Neuropharmacology 56* (Suppl 1), 3−8.
(27) Kahlig, K. M., Lute, B. J., Wei, Y., Loland, C. J., Gether, U., Javitch, J. A., and Galli, A. (2006) Regulation of dopamine transporter trafficking by intracellular amphetamine. *Mol. Pharmacol. 70*, 542−8.
(28) Bisagno, V., Gonzalez, B., and Urbano, F. J. (2016) Cognitive enhancers versus addictive psychostimulants: The good and bad side of dopamine on prefrontal cortical circuits. *Pharmacol. Res. 109*, 108−18.
(29) Schmeichel, B. E., Zemlan, F. P., and Berridge, C. W. (2013) A selective dopamine reuptake inhibitor improves prefrontal cortex-dependent cognitive function: potential relevance to attention deficit hyperactivity disorder. *Neuropharmacology 64*, 321−8.
(30) Giros, B., Jaber, M., Jones, S. R., Wightman, R. M., and Caron, M. G. (1996) Hyperlocomotion and indifference to cocaine and amphetamine in mice lacking the dopamine transporter. *Nature 379*, 606−12.
(31) Zahniser, N. R., and Sorkin, A. (2004) Rapid regulation of the dopamine transporter: role in stimulant addiction? *Neuropharmacology 47* (Suppl 1), 80−91.
(32) Volkow, N. D., Wang, G. J., Fischman, M. W., Foltin, R. W., Fowler, J. S., Abumrad, N. N., Vitkun, S., Logan, J., Gatley, S. J., Pappas, N., Hitzemann, R., and Shea, C. E. (1997) Relationship between subjective effects of cocaine and dopamine transporter occupancy. *Nature 386*, 827−30.
(33) Carroll, F. I., Blough, B. E., Abraham, P., Mills, A. C., Holleman, J. A., Wolckenhauer, S. A., Decker, A. M., Landavazo, A., McElroy, K. T., Navarro, H. A., Gatch, M. B., and Forster, M. J. (2009) Synthesis and biological evaluation of bupropion analogues as potential pharmacotherapies for cocaine addiction. *J. Med. Chem. 52*, 6768−81.
(34) Vosburg, S. K., Hart, C. L., Haney, M., Rubin, E., and Foltin, R. W. (2010) Modafinil does not serve as a reinforcer in cocaine abusers. *Drug Alcohol Depend. 106*, 233−6.
(35) Desai, R. I., Kopajtic, T. A., Koffarnus, M., Newman, A. H., and Katz, J. L. (2005) Identification of a dopamine transporter ligand that blocks the stimulant effects of cocaine. *J. Neurosci. 25*, 1889−93.
(36) Schmitt, K. C., Rothman, R. B., and Reith, M. E. (2013) Nonclassical pharmacology of the dopamine transporter: atypical inhibitors, allosteric modulators, and partial substrates. *J. Pharmacol. Exp. Ther. 346*, 2−10.
(37) Li, Y. H., Wang, P. P., Li, X. X., Yu, C. Y., Yang, H., Zhou, J., Xue, W. W., Tan, J., and Zhu, F. (2016) The human kinome targeted by FDA approved multi-target drugs and combination products: A comparative study from the drug-target interaction network perspective. *PLoS One 11*, e0165737.
(38) Loland, C. J., Desai, R. I., Zou, M. F., Cao, J., Grundt, P., Gerstbrein, K., Sitte, H. H., Newman, A. H., Katz, J. L., and Gether, U. (2008) Relationship between conformational changes in the dopamine transporter and cocaine-like subjective effects of uptake inhibitors. *Mol. Pharmacol. 73*, 813−23.
(39) Loland, C. J., Norregaard, L., Litman, T., and Gether, U. (2002) Generation of an activating $Zn(2^+)$ switch in the dopamine transporter: mutation of an intracellular tyrosine constitutively alters the conformational equilibrium of the transport cycle. *Proc. Natl. Acad. Sci. U. S. A. 99*, 1683−8.
(40) Schmitt, K. C., and Reith, M. E. (2011) The atypical stimulant and nootropic modafinil interacts with the dopamine transporter in a different manner than classical cocaine-like inhibitors. *PLoS One 6*, e25790.
(41) Beuming, T., Kniazeff, J., Bergmann, M. L., Shi, L., Gracia, L., Raniszewska, K., Newman, A. H., Javitch, J. A., Weinstein, H., Gether, U., and Loland, C. J. (2008) The binding sites for cocaine and dopamine in the dopamine transporter overlap. *Nat. Neurosci. 11*, 780−9.
(42) Di Meo, F., Fabre, G., Berka, K., Ossman, T., Chantemargue, B., Paloncyova, M., Marquet, P., Otyepka, M., and Trouillas, P. (2016) In silico pharmacology: Drug membrane partitioning and crossing. *Pharmacol. Res. 111*, 471−86.
(43) Li, B., Tang, J., Yang, Q., Cui, X., Li, S., Chen, S., Cao, Q., Xue, W., Chen, N., and Zhu, F. (2016) Performance evaluation and online

DOI: 10.1021/acschemneuro.7b00173
ACS Chem. Neurosci. 2017, 8, 1416−1428

realization of data-driven normalization methods used in lc/ms based untargeted metabolomics analysis. *Sci. Rep. 6*, 38881.
(44) Tao, L., Zhu, F., Xu, F., Chen, Z., Jiang, Y. Y., and Chen, Y. Z. (2015) Co-targeting cancer drug escape pathways confers clinical advantage for multi-target anticancer drugs. *Pharmacol. Res. 102*, 123−31.
(45) Zheng, G., Xue, W., Wang, P., Yang, F., Li, B., Li, X., Li, Y., Yao, X., and Zhu, F. (2016) Exploring the inhibitory mechanism of approved selective norepinephrine reuptake inhibitors and reboxetine enantiomers by molecular dynamics study. *Sci. Rep. 6*, 26883.
(46) Coleman, J. A., Green, E. M., and Gouaux, E. (2016) X-ray structures and mechanism of the human serotonin transporter. *Nature 532*, 334−9.
(47) Wang, K. H., Penmatsa, A., and Gouaux, E. (2015) Neurotransmitter and psychostimulant recognition by the dopamine transporter. *Nature 521*, 322−7.
(48) Sund-Levander, M., and Grodzinsky, E. (2013) Assessment of body temperature measurement options. *Br. J. Nursing 22*, 942.
(49) Yang, F., Fu, T., Zhang, X., Hu, J., Xue, W., Zheng, G., Li, B., Li, Y., Yao, X., and Zhu, F. (2017) Comparison of computational model and X-ray crystal structure of human serotonin transporter: potential application for the pharmacology of human monoamine transporters. *Mol. Simul.*, DOI: 10.1080/08927022.2017.1309653.
(50) Li, Y. H., Xu, J. Y., Tao, L., Li, X. F., Li, S., Zeng, X., Chen, S. Y., Zhang, P., Qin, C., Zhang, C., Chen, Z., Zhu, F., and Chen, Y. Z. (2016) SVM-Prot 2016: A web-server for machine learning prediction of protein functional families from sequence irrespective of similarity. *PLoS One 11*, e0155290.
(51) Loland, C. J., Mereu, M., Okunola, O. M., Cao, J., Prisinzano, T. E., Mazier, S., Kopajtic, T., Shi, L., Katz, J. L., Tanda, G., and Newman, A. H. (2012) R-modafinil (armodafinil): a unique dopamine uptake inhibitor and potential medication for psychostimulant abuse. *Biol. Psychiatry 72*, 405−13.
(52) Bymaster, F. P., Katner, J. S., Nelson, D. L., Hemrick-Luecke, S. K., Threlkeld, P. G., Heiligenstein, J. H., Morin, S. M., Gehlert, D. R., and Perry, K. W. (2002) Atomoxetine increases extracellular levels of norepinephrine and dopamine in prefrontal cortex of rat: a potential mechanism for efficacy in attention deficit/hyperactivity disorder. *Neuropsychopharmacology 27*, 699−711.
(53) Williard, R. L., Middaugh, L. D., Zhu, H. J., and Patrick, K. S. (2007) Methylphenidate and its ethanol transesterification metabolite ethylphenidate: brain disposition, monoamine transporters and motor activity. *Behav. Pharmacol. 18*, 39−51.
(54) Simmler, L. D., Buser, T. A., Donzelli, M., Schramm, Y., Dieu, L. H., Huwyler, J., Chaboz, S., Hoener, M. C., and Liechti, M. E. (2013) Pharmacological characterization of designer cathinones in vitro. *Br. J. Pharmacol. 168*, 458−70.
(55) Oakes, T. M., Dellva, M. A., Waterman, K., Greenbaum, M., Poppe, C., Goldberger, C., Ahl, J., and Perahia, D. G. (2015) Edivoxetine compared to placebo as adjunctive therapy to selective serotonin reuptake inhibitors in the prevention of symptom re-emergence in major depressive disorder. *Curr. Med. Res. Opin. 31*, 1179−89.
(56) Wang, J., Morin, P., Wang, W., and Kollman, P. A. (2001) Use of MM-PBSA in reproducing the binding free energies to HIV-1 RT of TIBO derivatives and predicting the binding mode to HIV-1 RT of efavirenz by docking and MM-PBSA. *J. Am. Chem. Soc. 123*, 5221−30.
(57) Reyes, C. M., and Kollman, P. A. (2000) Structure and thermodynamics of RNA-protein binding: using molecular dynamics and free energy analyses to calculate the free energies of binding and conformational change. *J. Mol. Biol. 297*, 1145−58.
(58) Hou, T., Wang, J., Li, Y., and Wang, W. (2011) Assessing the performance of the MM/PBSA and MM/GBSA methods. 1. The accuracy of binding free energy calculations based on molecular dynamics simulations. *J. Chem. Inf. Model. 51*, 69−82.
(59) Genheden, S., and Ryde, U. (2015) The MM/PBSA and MM/GBSA methods to estimate ligand-binding affinities. *Expert Opin. Drug Discovery 10*, 449−61.
(60) Chen, F., Liu, H., Sun, H., Pan, P., Li, Y., Li, D., and Hou, T. (2016) Assessing the performance of the MM/PBSA and MM/GBSA methods. 6. Capability to predict protein-protein binding free energies and re-rank binding poses generated by protein-protein docking. *Phys. Chem. Chem. Phys. 18*, 22129−39.
(61) Sun, H., Li, Y., Tian, S., Wang, J., and Hou, T. (2014) P-loop conformation governed crizotinib resistance in G2032R-mutated ROS1 tyrosine kinase: clues from free energy landscape. *PLoS Comput. Biol. 10*, e1003729.
(62) Xu, L., Zhang, Y., Zheng, L., Qiao, C., Li, Y., Li, D., Zhen, X., and Hou, T. (2014) Discovery of novel inhibitors targeting the macrophage migration inhibitory factor via structure-based virtual screening and bioassays. *J. Med. Chem. 57*, 3737−45.
(63) Schmitt, K. C., Mamidyala, S., Biswas, S., Dutta, A. K., and Reith, M. E. (2010) Bivalent phenethylamines as novel dopamine transporter inhibitors: evidence for multiple substrate-binding sites in a single transporter. *J. Neurochem. 112*, 1605−18.
(64) Sorensen, L., Andersen, J., Thomsen, M., Hansen, S. M., Zhao, X., Sandelin, A., Stromgaard, K., and Kristensen, A. S. (2012) Interaction of antidepressants with the serotonin and norepinephrine transporters: mutational studies of the S1 substrate binding pocket. *J. Biol. Chem. 287*, 43694−707.
(65) Andersen, J., Ringsted, K. B., Bang-Andersen, B., Stromgaard, K., and Kristensen, A. S. (2015) Binding site residues control inhibitor selectivity in the human norepinephrine transporter but not in the human dopamine transporter. *Sci. Rep. 5*, 15650.
(66) Abramyan, A. M., Stolzenberg, S., Li, Z., Loland, C. J., Noe, F., and Shi, L. (2017) The isomeric preference of an atypical dopamine transporter inhibitor contributes to its selection of the transporter conformation. *ACS Chem. Neurosci.*, DOI: 10.1021/acschemneuro.7b00094.
(67) Paulson, J. N., Stine, O. C., Bravo, H. C., and Pop, M. (2013) Differential abundance analysis for microbial marker-gene surveys. *Nat. Methods 10*, 1200−2.
(68) Ward, L. F., Enders, J. R., Bell, D. S., Cramer, H. M., Wallace, F. N., and McIntire, G. L. (2016) Improved chiral separation of methamphetamine enantiomers using CSP-LC-MS-MS. *J. Anal. Toxicol. 40*, 255−63.
(69) Khan, A., and Reinhard, J. F., Jr. Compositions and methods for treating depression, adhd and other central nervous system disorders employing novel bupropion compounds, and methods for production and use of novel bupropion compounds and formulations. Patent WO2012118562A1, 7 September, 2012.
(70) Maneeton, B., Maneeton, N., Likhitsatian, S., Suttajit, S., Narkpongphun, A., Srisurapanont, M., and Woottiluk, P. (2015) Comparative efficacy, acceptability, and tolerability of lisdexamfetamine in child and adolescent ADHD: a meta-analysis of randomized, controlled trials. *Drug Des., Dev. Ther. 9*, 1927−36.
(71) Larkin, M. A., Blackshields, G., Brown, N. P., Chenna, R., McGettigan, P. A., McWilliam, H., Valentin, F., Wallace, I. M., Wilm, A., Lopez, R., Thompson, J. D., Gibson, T. J., and Higgins, D. G. (2007) Clustal W and Clustal X version 2.0. *Bioinformatics 23*, 2947−8.
(72) Arnold, K., Bordoli, L., Kopp, J., and Schwede, T. (2006) The SWISS-MODEL workspace: a web-based environment for protein structure homology modelling. *Bioinformatics 22*, 195−201.
(73) Yamashita, A., Singh, S. K., Kawate, T., Jin, Y., and Gouaux, E. (2005) Crystal structure of a bacterial homologue of Na^+/Cl^--dependent neurotransmitter transporters. *Nature 437*, 215−23.
(74) Vaguine, A. A., Richelle, J., and Wodak, S. J. (1999) SFCHECK: a unified set of procedures for evaluating the quality of macromolecular structure-factor data and their agreement with the atomic model. *Acta Crystallogr., Sect. D: Biol. Crystallogr. 55*, 191−205.
(75) Wang, P., Yang, F., Yang, H., Xu, X., Liu, D., Xue, W., and Zhu, F. (2015) Identification of dual active agents targeting 5-HT1A and SERT by combinatorial virtual screening methods. *Bio-Med. Mater. Eng. 26* (Suppl 1), S2233−9.
(76) Schrödinger, L. (2010) *The PyMOL Molecular Graphics System*, version 1.3, Schrödinger, LLC, New York.

DOI: 10.1021/acschemneuro.7b00173
ACS Chem. Neurosci. 2017, 8, 1416−1428

(77) Schrödinger, L. (2009) *Glide*, version 5.5, Schrödinger, LLC, New York.
(78) Xue, W., Wang, P., Li, B., Li, Y., Xu, X., Yang, F., Yao, X., Chen, Y. Z., Xu, F., and Zhu, F. (2016) Identification of the inhibitory mechanism of FDA approved selective serotonin reuptake inhibitors: an insight from molecular dynamics simulation study. *Phys. Chem. Chem. Phys. 18*, 3260−71.
(79) Wu, E. L., Cheng, X., Jo, S., Rui, H., Song, K. C., Davila-Contreras, E. M., Qi, Y., Lee, J., Monje-Galvan, V., Venable, R. M., Klauda, J. B., and Im, W. (2014) CHARMM-GUI Membrane Builder toward realistic biological membrane simulations. *J. Comput. Chem. 35*, 1997−2004.
(80) Hornak, V., Abel, R., Okur, A., Strockbine, B., Roitberg, A., and Simmerling, C. (2006) Comparison of multiple Amber force fields and development of improved protein backbone parameters. *Proteins: Struct., Funct., Genet. 65*, 712−25.
(81) AMBER (2014) *AMBER*, version 14, University of California, San Francisco.
(82) Koldso, H., Autzen, H. E., Grouleff, J., and Schiott, B. (2013) Ligand induced conformational changes of the human serotonin transporter revealed by molecular dynamics simulations. *PLoS One 8*, e63635.
(83) Hara, Y., and Murayama, S. (1992) Effects of analgesic-antipyretics on the spinal reflex potentials in cats: an analysis of the excitatory action of aminopyrine. *Nippon Yakurigaku Zasshi 100*, 383−90.
(84) Springborg, M., and Kirtman, B. (2007) Efficient vector potential method for calculating electronic and nuclear response of infinite periodic systems to finite electric fields. *J. Chem. Phys. 126*, 104107.
(85) Massova, I., and Kollman, P. A. (2000) Combined molecular mechanical and continuum solvent approach (MM-PBSA_GBSA) to predict ligand. *Perspect. Drug Discovery Des. 18*, 113−135.
(86) Xu, L., Sun, H., Li, Y., Wang, J., and Hou, T. (2013) Assessing the performance of MM/PBSA and MM/GBSA methods. 3. The impact of force fields and ligand charge models. *J. Phys. Chem. B 117*, 8408−21.
(87) Sun, H., Li, Y., Tian, S., Xu, L., and Hou, T. (2014) Assessing the performance of MM/PBSA and MM/GBSA methods. 4. Accuracies of MM/PBSA and MM/GBSA methodologies evaluated by various simulation protocols using PDBbind data set. *Phys. Chem. Chem. Phys. 16*, 16719−29.
(88) Sun, H., Li, Y., Shen, M., Tian, S., Xu, L., Pan, P., Guan, Y., and Hou, T. (2014) Assessing the performance of MM/PBSA and MM/GBSA methods. 5. Improved docking performance using high solute dielectric constant MM/GBSA and MM/PBSA rescoring. *Phys. Chem. Chem. Phys. 16*, 22035−45.
(89) Froesner, G. G., Peterson, D. A., Deinhardt, F. W., and Holmes, A. W. (1973) Transmission of hepatitis A and hepatitis B by shared needle. *Lancet 301*, 1183.
(90) Weiser, J., Shenkin, P. S., and Clark Still, W. (1999) Approximate atomic surfaces from linear combinations of pairwise overlaps (LCPO). *J. Comput. Chem. 20*, 217−230.
(91) Tippmann, S. (2015) Programming tools: Adventures with R. *Nature 517*, 109−10.
(92) Barer, M. R., and Harwood, C. R. (1999) Bacterial viability and culturability. *Adv. Microb. Physiol. 41*, 93−137.
(93) Letunic, I., and Bork, P. (2007) Interactive Tree Of Life (iTOL): an online tool for phylogenetic tree display and annotation. *Bioinformatics 23*, 127−8.

DOI: 10.1021/acschemneuro.7b00173
ACS Chem. Neurosci. 2017, 8, 1416−1428